Sensitivity of CFS Mean State and ENSO Variability to Changes in SST Bias

Julia V. Manganello[1,*] and Bohua Huang[1,2]

[1] *Center for Ocean-Land-Atmosphere Studies, Calverton MD*
[2] *Climate Dynamics Department, College of Science*
George Mason University, Fairfax, VA

NOAA CTB - COLA
Joint Seminar
Mar. 12, 2008

1. Introduction

Tropical biases, including the Southeast Pacific (SEP) warm SST bias, have persisted in coupled general circulation models (CGCMs) for quite some time. It is generally believed that this tropical warm bias is a major factor that limits the interannual variability and predictability in current CGCMs (Li and Hogan 1999, Wittenberg et al. 2006, Manganello and Huang 2008). Therefore, it is important to understand its specific effects in the coupled systems.

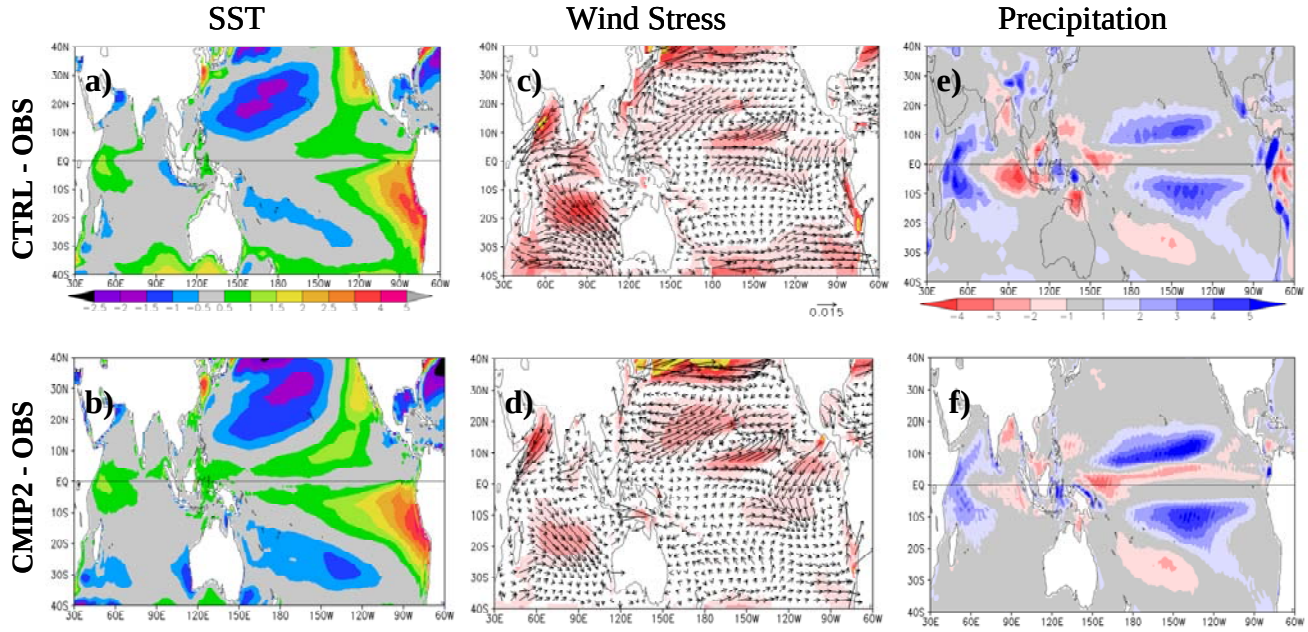

Figure 1 *Left Panel*: annual mean SST errors from the (a) fully coupled integration with CFS03 at T62L64 (CTRL) and (b) CMIP2 simulation relative to CPC SST data for 1950-2001. Units are °C. *Middle Panel*: annual mean surface wind stress errors from the (c) CTRL and (d) CMIP2 relative to ERS-1 data for 1991-2000. The arrow is 0.015 N/m^2, representing the unit vector. Shading indicates large magnitudes of error vector. *Right Panel*: annual mean precipitation error from the (e) CTRL and (f) CMIP2 relative to CMAP data for 1979-2005. Units are mm/day.

In the NCEP Climate Forecast System (CFS; Saha et al. 2006), SEP SST error reaches about 2-3°C (Fig. 1a) and is one of the largest in the Tropics. Associated with this error, surface wind stress shows an erroneous convergence over the region. Near the coast, the warm SST bias persists against the cooling effects of intensive evaporation and coastal upwelling induced by the overly strong alongshore southerlies (Fig. 1c). A wet bias in the SEP is consistent with the above-mentioned SST and wind stress errors (Fig. 1e). In general, CFS shows a double-ITCZ signature, where excessive precipitation is observed both north and south of the equator throughout the central and eastern Pacific. In the Indian Ocean the center of precipitation is shifted westward away from the Sumatra coast. Correspondingly, the Indian Ocean equatorial winds are too easterly while the off-

*Correspondence to: Julia V. Manganello, Center for Ocean-Land-Atmosphere Studies, 4041 Powder Mill Road, Suite 302, Calverton, MD 20705; E-mail: julia@cola.iges.org

equatorial southeasterly trade winds are too weak. In the CMIP2 integration with a new version of CFS at T126L64, Indian Ocean errors are reduced but the tropical Pacific biases are still present and are of the same magnitude, if not larger, with the exception of the coastal wind errors off South America (Figs. 1b, d and f). It further confirms that the coastal wind bias in CFS is an independent problem from the SEP SST bias because the latter persists without the coastal wind bias.

In this study, we present results from a set of heat and momentum flux correction experiments (HFC and MFC hereafter) that were designed to empirically reduce tropical SST biases in CFS. In the HFC experiment, heat flux correction term that was added to the surface heat flux into the ocean was set to vary spatially but remain constant in time. Its magnitude was proportional to the annual mean local SST error from the 52-year long fully coupled CFS integration (CTRL). Proportionality factor was set everywhere to -15 W/m^2/K. Furthermore, heat flux correction was restricted only to the SEP and the Southeast Atlantic where SST errors were larger than 1.5 °C. In the MFC experiment, momentum flux correction term was set to be equal to the annual mean CFS surface wind stress errors with respect to the remotely sensed scatterometer ERS-1 wind stress for the period of 1991-2001, taken with a negative sign. The correction was restricted to 30°S-30°N, tapering off to zero at 40°S and 40°N. In both HFC and MFC experiments, CFS was integrated for 115 years starting from January 1, 1985 initial conditions with their corresponding corrections. Outputs from the last 100 years of each run were used for the analysis.

2. Mean climate in the tropical Pacific

HFC is found to be successful in reducing SEP SST bias and the associated precipitation bias, practically eliminating CFS precipitation errors in the South Pacific east of the dateline (Figs. 2a and 2c). However, these changes produce new errors in the model: cold SST bias at the equator and in the central South Pacific (Fig. 2a); stronger equatorial easterlies and southeasterlies compared to observations and further weakening of northeasterlies in the eastern Pacific with respect to the CTRL (Figs. 1c and 2b); as well as larger wet bias over the ITCZ compared to the CTRL (Figs. 1e and 2c).

According to the heat budget analysis, the cold SST errors south of the equator are a remote response to the heat flux correction and are due to cooling by anomalous Ekman transport in response to surface wind stress changes. On the other hand, the amplification of the wet bias in the ITCZ is likely due to increased divergence out of the SEP in the lower troposphere and the subsequent enhancement of moisture flux convergence over the ITCZ. To some extent, this response is expected as warm SST bias is reduced, which leads to reduction in convection and increase in sea level pressure (SLP), as well as the northward cross-equatorial flow. Since the precipitation in the northern branch of the double ITCZ is already excessive in CFS, the increased convergence inevitably amplifies this bias. The presence of overly active ITCZ could be traced to Global Forecast System (GFS), which is the atmospheric component of CFS. In fact, the wet ITCZ bias in the HFC is similar in magnitude to the corresponding bias in the AMIP-type simulation with GFS (not

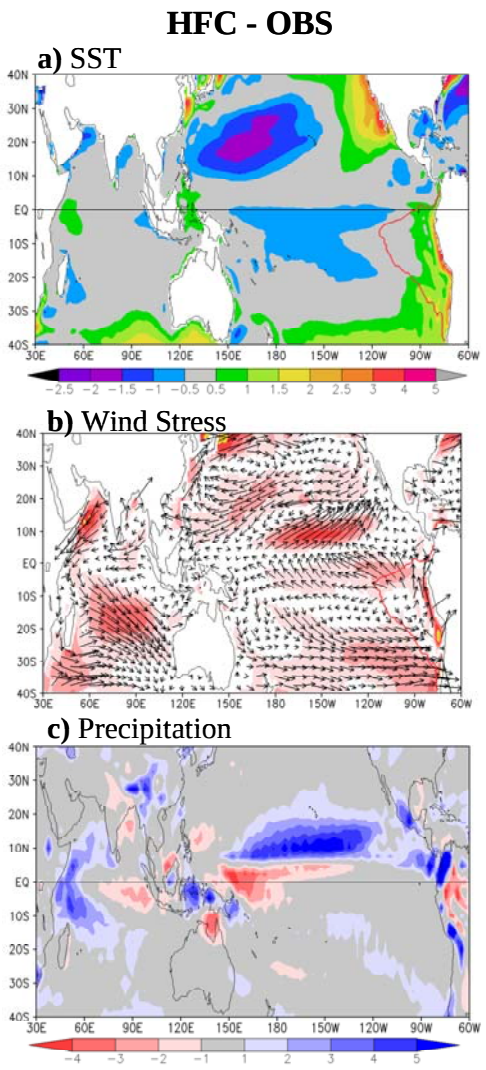

Figure 2 Annual mean errors of (a) SST, (b) surface wind stress and (c) precipitation from the HFC relative to CPC SST data for 1950-2001, ERS-1 data for 1991-2000 and CMAP data for 1979-2005 respectively. Units are °C and red contour shows the extent of heat flux correction in (a). In (b) the arrow is 0.015 N/m^2, representing the unit vector. Shading indicates large magnitudes of error vector. Units are mm/day in (c).

shown). Weakening of the northeasterly surface wind stress in the eastern Pacific is directly linked to these ITCZ errors.

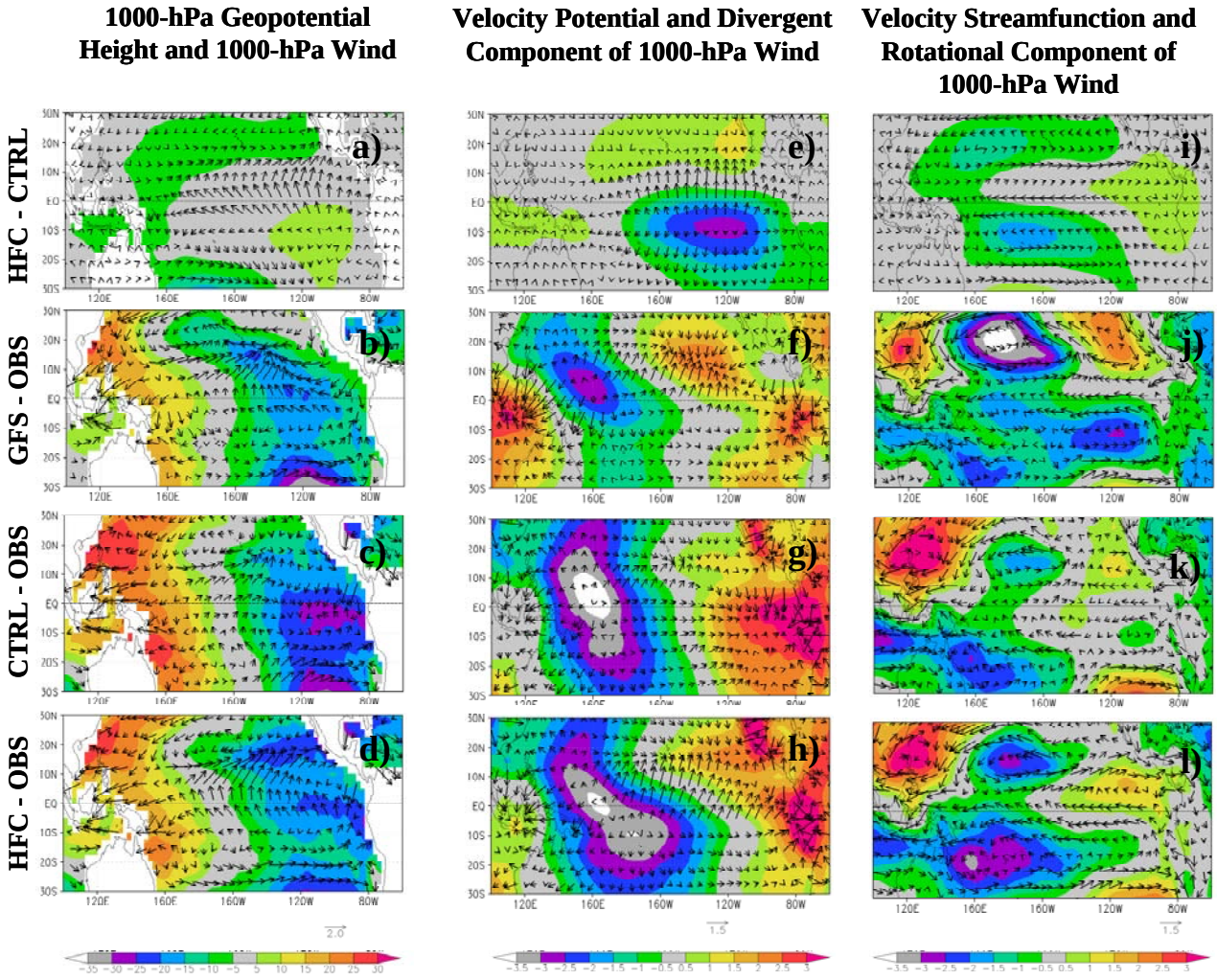

Figure 3 *Left Panel:* 1000-hPa geopotential height and 1000-hPa wind (a) response to the HFC; bias in the (b) GFS AMIP run, 1961-2002, (c) CTRL and (d) HFC relative to the NCEP/DOE Reanalsys-2 (R2). *Middle Panel:* velocity potential and divergent component of the 1000-hPa wind (e) response to the HFC; bias in the (f) GFS AMIP run, 1961-2002, (g) CTRL and (h) HFC relative to the R2. *Right Panel:* velocity streamfunction and rotational component of the 1000-hPa wind (i) response to the HFC; bias in the (j) GFS AMIP run, 1961-2002, (k) CTRL and (l) HFC relative to the R2. Units are m, m/s and 10^6 m^2/s. The unit vectors are 2.0, 1.5 and 1.5 m/s respectively.

It is critical to understand the origin of the easterly wind bias at the equator in the HFC since the related cold SST bias could adversely affect El Niño-Southern Oscillation (ENSO) feedbacks by shifting the precipitation and wind stress anomalies westward, which could also change some properties of ENSO (e.g. Kirtman 1997, An and Wang 2000, Wittenberg et al. 2006). For this purpose, we decompose the summer-average (JJA) 1000-hPa wind response to the heat flux correction and the respective model bias into the divergent and rotational components (Fig. 3). (Analysis of the winter means leads to similar conclusions). First of all, equatorial easterly wind bias is already present in the GFS AMIP-type simulation and is due to rotational wind errors as a result of a large-scale too strong anti-cyclonic circulation present in the Southern Hemisphere Tropics (Figs. 3b, f and j). In the coupled mode (CTRL), the equatorial easterly wind is reduced. In fact, the equatorial wind bias becomes weakly westerly mostly as a result of additional convergence over the SEP because of low SLP bias there (associated with the warm SSTs), as rotational wind errors are weakened (Figs. 3e, g and k). Therefore, the

presence of the warm bias cancels out some of the model errors associated with an overly strong model ITCZ. In HFC, however, reduced SEP SST bias again increases regional SLP and the southeast trades. This change reinforces the anti-cyclonic circulation in the south Pacific and re-creates easterly wind bias at the equator to the level largely similar to the GFS AMIP run (Figs. 3d, h and l). (Divergent wind errors in the HFC actually lead to weaker equatorial easterlies (Fig. 3h)). The similarity between GFS AMIP and HFC experiments is rather astonishing. We therefore conclude that reducing SEP SST bias in CFS could expose and amplify other systematic errors that originate from the atmospheric component of CFS and appear to be related to an overly active ITCZ.

3. Mean climate in the Indian Ocean

The largest benefit of the MFC for the mean climate is found in the Indian Ocean. Since the overly strong alongshore winds off the Peru coast tend to cool the ocean down, reducing large southerly bias of alongshore winds in the SEP amplifies the existing warm SST bias by about 1.5°C near the coast and 0.5°C in the tropical Pacific.

The most significant effect of the momentum flux correction in the Indian Ocean amounts to reducing equatorial and coastal upwelling and improving upper ocean temperature distribution at the equator. As a result, the dipole errors in the SST and precipitation in the Indian Ocean (Figs. 1a and e) become much smaller (not shown).

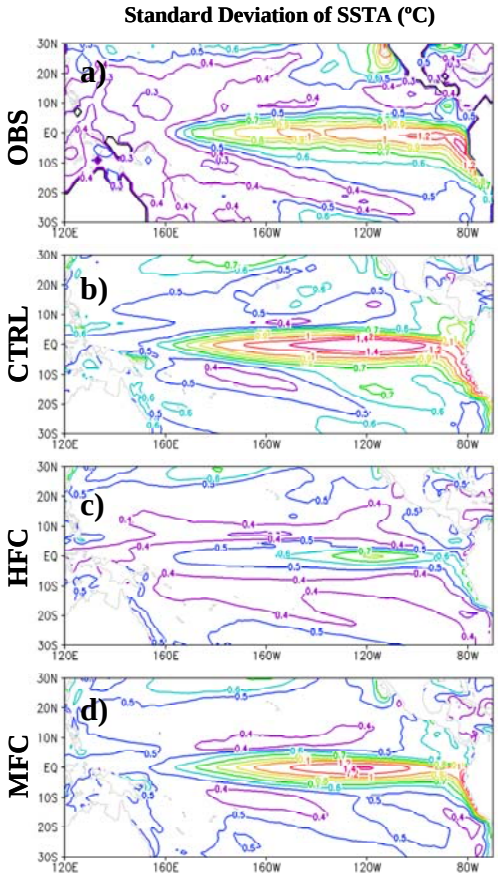

Figure 4 Standard deviation of the interannual SST anomalies from (a) CPC SST data for 1950-2001, the (b) CTRL, (c) HFC and (d) MFC experiments. Units are °C.

4. El Niño-Southern Oscillation

ENSO in CFS is found to exhibit a high degree of sensitivity to the mean state changes imposed by heat and momentum flux corrections. In HFC, the variance of interannual SST anomalies (SSTA) in the equatorial Pacific is considerably reduced (Fig. 4c) and is barely statistically significant over the Niño-3.4 region (Fig. 5a). On the other hand, in the MFC SSTA variance is generally more in line with the observations compared to the CTRL (Fig.4d). Besides weaker amplitude, ENSO is much less regular in this experiment (Fig. 5a). In addition, the duration of warm ENSO events is more realistic in both experiments, but more so in the MFC (Fig. 5b). It is found that the equatorial thermocline in the HFC is substantially deeper and more diffuse compared both to the CTRL and MFC, which could partly explain the loss of ENSO strength in this simulation (Meehl et al. 2001).

Zonal wind stress and precipitation responses to the Niño-3 SSTA also show certain differences. Although regression patterns in the HFC exhibit the highest degree of zonal asymmetry including the easterly wind response in the eastern equatorial Pacific (Figs. 6c and g), the bulk of the response is shifted to the west of the dateline likely due to the equatorial cold SST bias, where it is slightly east of the dateline in the observations (Figs. 6a and e). This change could in turn shift the subsurface response westward away from the region of strong air-sea coupling. Regression of subsurface temperature onto the Niño-3 Index (not shown) indicates that indeed in the eastern equatorial Pacific subsurface temperature variability is much weaker in the HFC compared to other simulations. The center of variability is located further westward, and the mixing appears to occur more along the isopycnals, rather than across them, and deeper than in the CTRL and MFC. Notable difference in the regression patterns of zonal wind stress in the MFC vs. CTRL is significant reduction of anomalous easterlies to the west of 160°E north of the equator (Figs. 6f and h). This change could be responsible for the increase in ENSO irregularity in the MFC according to Wang et al. (2005)

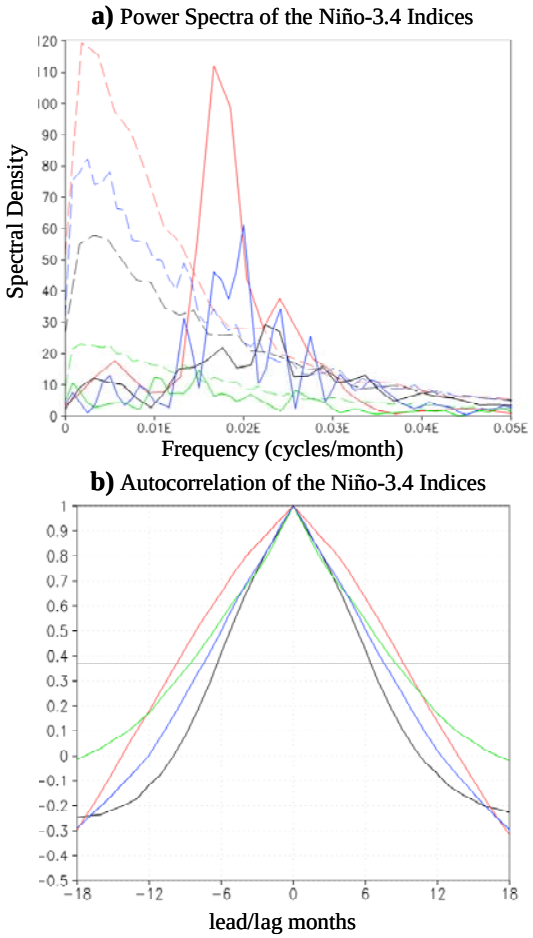

Figure 5 (a) Power spectra and (b) autocorrelation of the Niño-3.4 indices (SST anomalies averaged over 5°S-5°N, 120°-170°W) from the CPC SST data for 1950-2001 (black), the CTRL (red), HFC (green) and MFC (blue). Dashed lines in the upper plot indicate 95% significance levels.

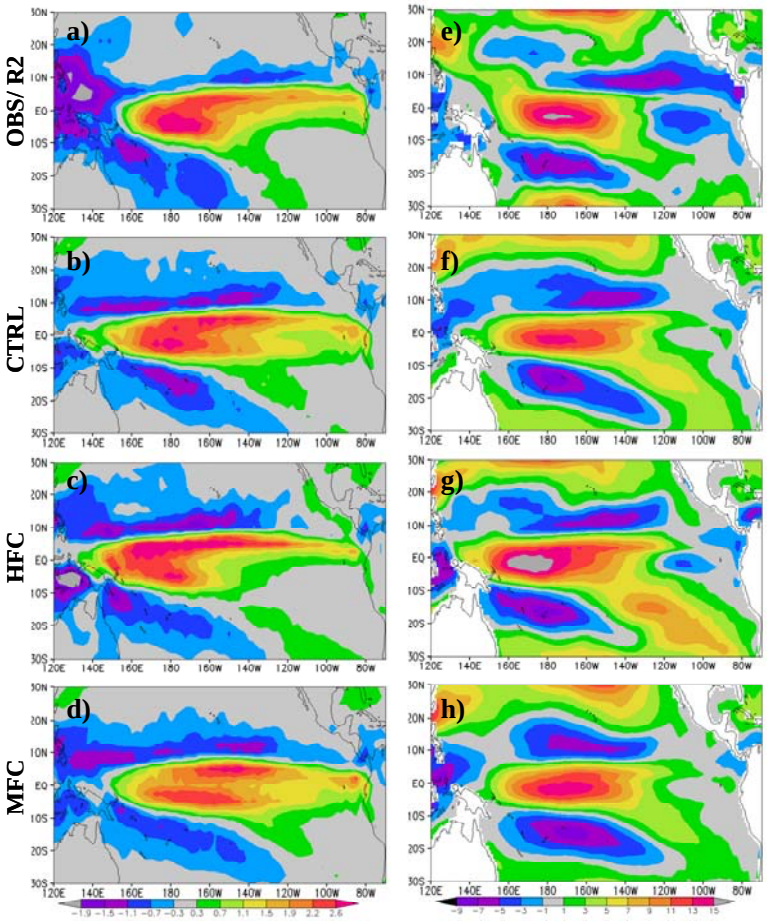

Figure 6 Linear regression coefficient of monthly mean precipitation anomalies from (a) CMAP data for 1979-2001, (b) CTRL, (c) HFC, (d) MFC and zonal wind stress anomalies from (e) NCEP-DOE Reanalysis-2 for 1979-2001, (f) CTRL, (g) HFC and (h) MFC onto the Niño-3 Index from CPC SST data for 1979-2001 for (a) and (e) and respective model simulations otherwise. Units are mm/(day*°C) and 10^{-3} N/(m^2*°C).

5. Summary

Both the ocean-atmosphere mean circulation and its annual and interannual variability in CFS exhibit a high degree of sensitivity to the Southeast Pacific SST bias. Reduction of this bias generally increases regional sea level pressure and the southeast trade winds. This change, however, exposes and amplifies other systematic errors in CFS, such as an excessive cross-equatorial flow in the eastern Pacific, that appear to be related to an overly active ITCZ. As a result, the heat flux corrected model demonstrates too strong equatorial easterlies and further weakening of northeasterlies in the eastern Pacific. The ITCZ errors to a varying extent are also present in the AMIP-type simulation with GFS and probably not directly linked to the SST; SEP bias therefore acts as a means to compensate for them.

As a consequence of surface wind stress errors in the heat flux correction experiment, CFS develops a cold SST bias at the equator and the central South Pacific. Equatorial thermocline becomes too deep and diffuse. These changes have a major impact on the model's ENSO simulation, considerably reducing its amplitude.

Largest improvements in the simulation of the mean climate due to momentum flux correction are found over the Indian Ocean. Moreover, with the reduction of the mean errors in the surface wind stress, amplitude and duration of ENSO events become more realistic in this simulation than directly coupled CFS integration.

References

An, S.-I., and B. Wang, 2000: Interdecadal change of the structure of the ENSO mode and its impact on the ENSO frequency. *J. Climate*, **13**, 2044-2055.

Kirtman, B. P., 1997: Oceanic Rossby wave dynamics and the ENSO period in a coupled model. *J. Climate*, **10**, 1690-1704.

Li, T., and T. F. Hogan, 1999: The role of the annual-mean climate on seasonal and interannual variability of the Tropical Pacific in a coupled GCM. *J. Climate*, **12**, 780-792.

Manganello, J. V., and B. Huang, 2008: The influence of systematic errors in the Southeast Pacific on ENSO variability and prediction in a Coupled GCM. *Clim. Dyn.* DOI 10.1007/s00382-008-0407-5 (available online).

Meehl, G. A., P. R. Gent, J. M. Arblaster, B. L. Otto-Bliesner, E. C. Brady and A. Craig, 2001: Factors that affect the amplitude of El Niño in global coupled climate models. *Clim. Dyn.*, **17**, 515-526.

Wang, W., S. Saha, H.-L. Pan, S. Nadiga and G. White, 2005: Simulation of NESO in the new NCEP Coupled Forecast System model (CFS03). *Mon. Wea. Rev.*, **133**, 1574-1593.

Wittenberg, A. T., A. Rosati, N.-C. Lau, and J. J. Ploshay, 2006: GFDL's CM2 global coupled climate models. Part III: Tropical Pacific climate and ENSO. *J. Climate*, **19**, 698-722.